Journal of Molecular Spectroscopy 348 (2018) 124–129

Contents lists available at ScienceDirect

Journal of Molecular Spectroscopy

journal homepage: www.elsevier.com/locate/jms

# Vibrational dynamic and spectroscopic molecular parameters of *trans*-Methylglyoxal, a gaseous precursor of secondary organic aerosols

S. Bteich, M. Goubet *, R.A. Motiyenko, L. Margulès, T.R. Huet

*Univ. Lille, CNRS, UMR8523 - PhLAM - Physique des Lasers Atomes et Molécules, F-59000 Lille, France*

ARTICLE INFO

*Article history:*
Received 31 August 2017
In revised form 16 November 2017
Accepted 3 December 2017
Available online 6 December 2017

*Keywords:*
Rotational spectroscopy
Internal rotation
Secondary organic aerosols precursor

ABSTRACT

Methylglyoxal is a secondary product of oxidation of isoprene and as such one of the most abundant α-dicarbonyls present in the atmosphere. Due to its low vapor pressure, it is highly suspected to be a secondary organic aerosols precursor. The rotational spectrum of Methylglyoxal in its vibrational ground state has been reinvestigated in the 4–500 GHz range and fitted to instrumental accuracies using a model taking into account the methyl group internal rotation motion and with the support of quantum chemistry calculations. Reliability of the line assignments and extracted molecular parameters is confirmed by the good agreement between experiments and calculations.



## 1. Introduction

Several volatile organic compounds (VOCs) are emitted by biogenic and anthropogenic sources into the atmosphere. A very rich atmospheric chemistry is taking place in the troposphere. In particular, the oxidation of isoprene by OH and $NO_3$ is believed to yield to the production of methyl-nitroxy butenal, $C_5$ carbonyls, hydroxy-methylvinyl ketone, methylvinyl ketone and methacroleine [1]. Methylglyoxal ($CH_3C(O)CHO$) is a secondary product of oxidation and as such one of the most abundant α-dicarbonyls present in the atmosphere (8 Tg C/y). Due to its low vapor pressure, Methylglyoxal is highly suspected to be a secondary organic aerosols precursor. The spectroscopic information on Methylglyoxal is rather scarce. The structure of the most stable *trans* conformer has been determined in an electron diffraction study by Akishin et al. [2]. It is a prolate asymmetric top ($\kappa = -0.54$) belonging to the $C_s$ point group (*ab* symmetry plane). The microwave spectrum (8–40 GHz) was subsequently observed and analyzed by Dyllick-Brenzinger and Bauder [3]. Several lines were assigned to the vibrational ground state (GS), and a few to the two first excited states (ES), the C—C and $CH_3$ torsional modes, located at 90.2 (4.1) and 122.7(4.9) $cm^{-1}$, respectively. A large amplitude motion, associated with the internal rotation of the methyl top was observed. From the splittings between the A and E rotational transitions, the height of the barrier to internal rotation was estimated at a value of 269.1(3) $cm^{-1}$. The rotational constants have been determined for the A components of the GS, as well as the electric dipole moment components ($\mu_a$ = 0.1597(11) D, $\mu_b$ = 0.9620(7) D). More recently, Profeta et al. published a quantitative infrared intensity study of vapor-phase Methylglyoxal [4]. A complete vibrational assignment is presented, with the support of accurate quantum chemical calculations. The purpose of the present work is to obtain a set of molecular parameters characterizing the GS and the two first ES of *trans*-Methylglyoxal over a wide range of rotational energy levels. The set of molecular parameters could then be used to analyze infrared spectra recorded at high resolution in an infrared atmospheric window. To this end, it was necessary to extend the observed range of the rotational spectrum to the submillimeter-wave range and to use a global model to reproduce the torsion-rotation spectrum at the experimental accuracy. This approach was recently successfully applied to methacroleine and methylvinyl ketone, with the support of quantum chemistry calculations [5,6].

## 2. Laboratory methods

### 2.1. Chemical sample

A sample of 40% Methylglyoxal in water was purchased from Sigma–Aldrich. For jet-cooled experiments, the sample was used without further purification. For room temperature experiments, several cycles of cooling down the sample using liquid nitrogen and pumping over while heating gently up to room temperature

* Corresponding author.
*E-mail address:* manuel.goubet@univ-lille1.fr (M. Goubet).

https://doi.org/10.1016/j.jms.2017.12.007
0022-2852/

was performed in order to remove water as much as possible. In these conditions, Methylglyoxal was stable for a few hours, which was enough to record the spectra.

### 2.2. FP-FTMW spectroscopy experiment

In the present work, the Fabry-Pérot Fourier-transform microwave (FP-FTMW) technique coupled to a pulsed supersonic jet was used [7–9]. The jet-cooled pure rotation spectrum of Methylglyoxal was recorded in the frequency range 4–20 GHz using the supersonic jet FP-FTMW spectrometers of the PhLAM Laboratory in Lille [10,11]. A heated nozzle [12] allowed to mix the Methylglyoxal vapor with the carrier gas (neon) at a backing pressure of about 0.25 MPa. Temperatures ranging from 323 K to 353 K were found to optimize the signal-to-noise ratio (S/N) depending on the amplitude of the recorded lines. The mixture was introduced into a Fabry-Pérot cavity through a series 9 General Valve pin hole nozzle (0.8 mm) at a repetition rate of 1.5 Hz. Jet-cooled molecules ($T_{rot}$ of a few K) were polarized within the supersonic expansion by a 2 μs pulse. In our most recent setup, the free-induction decay (FID) signal is recorded using heterodyne detection at 30 MHz and digitized at a repetition rate of 120 MHz on a 14 bit resolution electronic card. FID signals were accumulated between 50 and 1000 times, depending on the line intensity, to obtain the best S/N. After transformation of the average time domain signals, lines of the amplitude spectrum were observed as Doppler doublets due to the coaxial arrangement of the jet and the Fabry-Pérot cavity. Each resonance frequency was measured as the average frequency of the two Doppler components. The spectral resolution is depending on the number of recorded points. The frequency grid was set to 1.84 kHz, which was found sufficient since the Doppler width of the lines should be of several kHz. Examples of observed signals are displayed in Fig. 1.

### 2.3. (sub)millimeter-wave spectroscopy experiment

The pure rotation spectrum of Methylglyoxal was also recorded in the frequency range 150–500 GHz using the (sub-)millimeter-wave spectrometer of the PhLAM Laboratory in Lille [13]. Briefly, the dried sample was vaporized at 298 K and the spectra were recorded at a static pressure of 30–45 μbar. The frequency of a reference source of radiation from the Agilent synthesizer (12.5–17.5 GHz) was first multiplied by six and amplified by a AMC-10 active sextupler from Virginia Diodes, Inc. (VDI). The power is high enough to use VDI passive Schottky diode-based multipliers (×2, ×3, ×5) in the next stage of the frequency multiplication chain. The frequency ranges 150–220 GHz, 225–330 GHz and 400–520 GHz were covered. The frequency steps were from 30 to 54 kHz with a duration between each step of 30 ms. The estimated uncertainties of the measured line frequencies are 50 kHz and 100 kHz depending on the S/N ratio, the observed line shape and the frequency range. Fig. 2 shows the mm-wave spectrum of Methylglyoxal around 185 GHz. It should be noted that we observed on the spectrum $H_2CO$ transitions, as a known impurity in the sample.

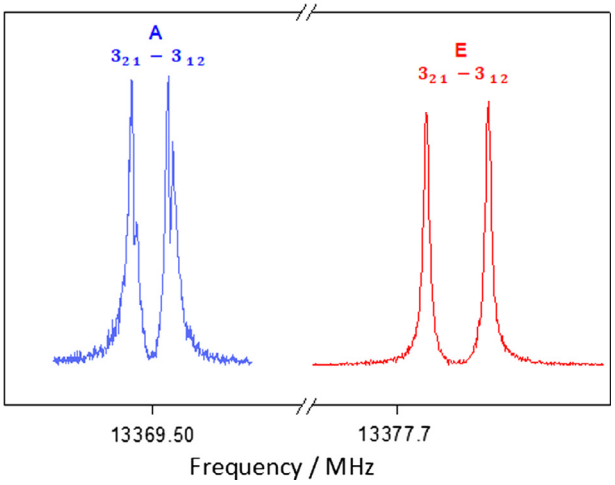


**Fig. 1.** Examples of high resolution FTMW lines (as Doppler doublets, see text) of *trans*-Methylglyoxal: A and E components of a $^b$Q-type transition (1000 accumulations). A typical spin-spin hyperfine structure is observed on the A component. Assignment is in the format $J'_{K'_aK'_c} - J''_{K''_aK''_c}$.

### 2.4. Computational details

All the calculations were performed using Gaussian 09 rev D.01 software [14] on the computing clusters of PhLAM laboratory. The frozen-core approximation was used throughout. Dunning and coworkers augmented correlation consistent basis set aug-cc-pVXZ (X = D, T, Q) were used (denoted hereafter aVDZ, aVTZ and aVQZ) [15]. All geometries were fully optimized at the MP2 and B98 levels using the tight convergence criterion. Extrapolations to complete basis set (CBS) for energies (including ZPE corrections) and rotational constants were performed from aVDZ, aVTZ and aVQZ results using Dunning's formula [16]. Frequencies and ground state (GS) rotational constants were calculated at the anharmonic level (VPT2 calculations as implemented in the Gaussian software [17]) with a tight SCF convergence criterion and the ultrafine integral grid option. Anharmonic corrections have been extrapolated from DFT (B98) to the MP2 level following a method suggested by Barone et al. [18] and recently successful in the case of systems containing carbonyl groups [19–21] (denoted "hybrid" hereafter). Briefly, since anharmonic calculations at the MP2 level are hardly affordable for such a relatively large molecule, rotational constants of a given vibrational state $v$ (called "hybrid") are estimated by adding DFT anharmonicity (B98/CBS) to the MP2 constants at equilibrium (MP2/CBS):

$$B_v^{hybrid} = B_{eq}^{MP2} - \left(B_{eq}^{B98} - B_v^{B98}\right) \quad (1)$$

where $B_v$ is the rotational constant of the vibrational state $v$ and $B_{eq}$ is the rotational constant at equilibrium.

## 3. Results and discussion

Methylglyoxal is a dicarbonyl molecule containing an aldehyde and a ketone group. *cis* and *trans* conformations, with respect to these two groups, are possible (see Fig. 3). However, only the *trans* conformer (denoted MG in the following) is expected to exist in the gas phase at room temperature as the *cis* conformer is estimated to lie at about 22 kJ/mol above in energy (MP2/aVQZ level). According to values of the dipole moment components (see introduction section), a b-type spectrum is expected with several a-type lines (the most intense ones). In particular, MG contains a methyl group with a barrier to internal rotation estimated to about 270 $cm^{-1}$. Consequently, each transition is split into two components of A and E symmetry, which are expected to be observed because of estimated separations from tens to hundreds of MHz largely higher than our spectrometers resolution. Hyperfine splittings due to spin-spin couplings have been observed for some lines (see e.g. component A in Fig. 1) but such features were too scarce to treat this coupling correctly in the present case.

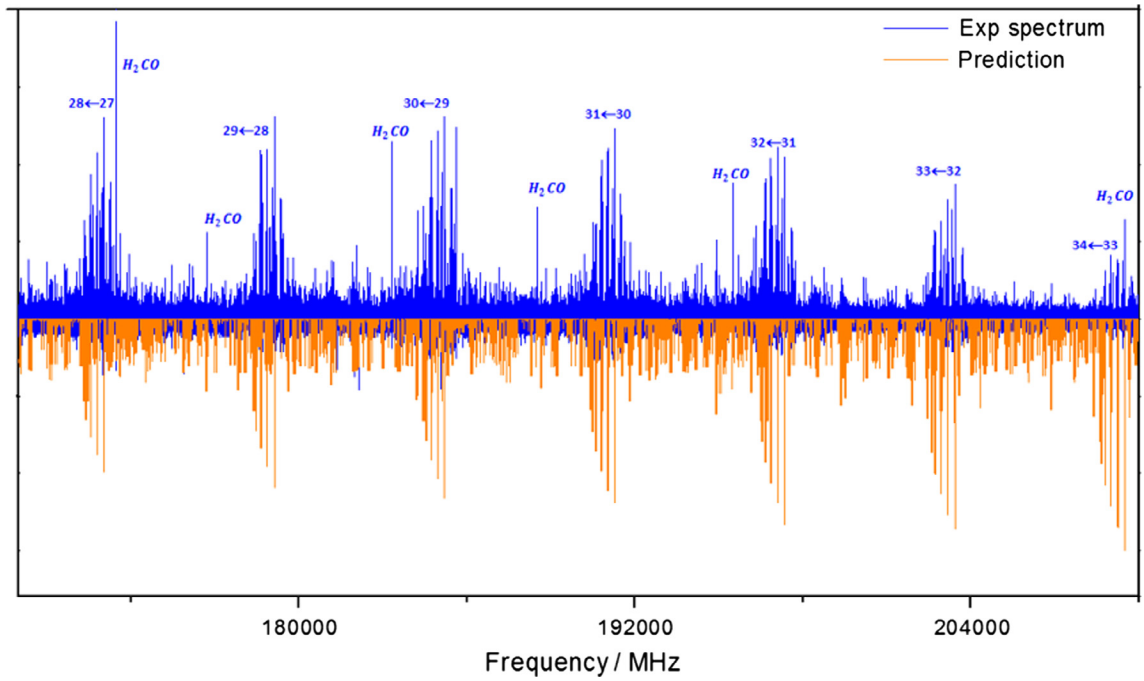


**Fig. 2.** Part of the mm-wave spectrum of *trans*-Methylglyoxal between 150 and 220 GHz, showing clusters of lines for a given *J* value: observed (in blue, upper trace) and simulated (in orange, lower trace) spectrum. Assignments are in the format $J' \leftarrow J''$. $H_2CO$ (as a known impurity in the sample) lines are also observed. (For interpretation of the references to color in this figure legend, the reader is referred to the web version of this article.)

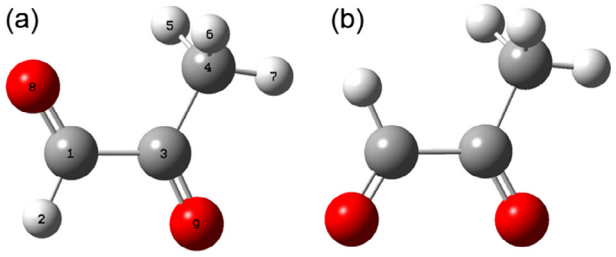


**Fig. 3.** Calculated equilibrium structures of Methylglyoxal (MP2/aVQZ): (a) *trans* (the most stable) and (b) *cis* (at about +22 kJ/mol) conformations relative to the aldehyde and ketone groups.

### 3.1. The rotational spectrum of trans-Methylglyoxal in its vibrational ground state

Analysis and fit of the rotational lines of MG in its vibrational GS have been performed using a three steps methodology briefly described in the following.

#### 3.1.1. First step

A rough initial analysis is performed using SPCAT/SPFIT suite [22]. Semi-rigid rotor parameters from the early study [3] have been used to predict the positions of A components with low *J* values in the cm-wave range. Experimental frequencies of the strongest $^{a}$R-type and $^{b}$R-type transitions have been rapidly assigned. Then, stepwise refinements of the fits were made including series of levels with higher quantum numbers values, Q-type transitions and different variations (from the lower to upper state of the transition) of $K_a$ and $K_c$. Although the use of a Watson-type Hamiltonian is obviously inappropriate in the case of MG, this first step permitted to unambiguously assign the A component of 22 new transitions.

#### 3.1.2. Second step

In order to include the E components to the analysis, a Hamiltonian taking into account the internal rotation motion should rather be used. The XIAM program [23] was chosen because its still relatively simple Hamiltonian (based on a Watson-type 1st order Hamiltonian) makes it very convenient to use during an explorative step. Starting from a prediction based on parameters from the above first step and a barrier height from [3], experimental frequencies of the E components of most of the cm-wave transitions have been rapidly assigned and fitted. Then, a new prediction extended to the mm-wave range could be generated, from which assignment of series of $^{b}$R-type transitions with low $K_a$ values (up to 4) was straightforward. However, XIAM is efficient for internal rotor with a medium to high barrier, which is not the case of MG. In addition, the number of distortion parameters associated with the internal rotation is limited, so its predictive power and fitting ability lack of accuracy when $K_a$ increases in a case such as MG. Therefore, a more appropriate model should be used to treat the submm-wave range.

#### 3.1.3. Third step

The RAM36 code, which proved its efficiency in the case of low barrier internal rotors [24,25], was then used for the final adjustment. Rotational constants and dipole moment components were converted from Principal Axis Method (PAM) system to Rho Axis Method (RAM) system used in RAM36, imposing to switch to the $II^{l}$ representation, using an angle $\theta_{RAM} = 12.83^{\circ}$ deduced from the MP2/aVQZ equilibrium structure. Although the RAM Hamiltonian is the correct model for MG, it converges slowly. Therefore, stepwise adjustments must be performed, introducing data as well as free parameters step by step for the beginning, even if confidence in the assignments was gained during the previous steps. Therefore, cm-wave lines, lines from [3] and series of $^{b}$R-type transitions with low $K_a$ values were first fitted to a limited number of parameters. Then, transitions involving higher $K_a$ values followed by ser-

**Table 1**
Ground state molecular parameters of *trans*-Methylglyoxal obtained using RAM36.

| Operator | $n_{tr}$[a] | Parameter | Value ($cm^{-1}$)[b] |
|---|---|---|---|
| $p_\alpha^2$ | $2_{20}$ | F | 5.471649399[c] |
| $p_\alpha P_a$ | $2_{11}$ | $\rho$ | 0.0292985(48) |
| $(1-\cos(3\alpha))$ | $2_{20}$ | $0.5V_3$ | 135.859(12) |
| $P_a^2$ | $2_{02}$ | A | 0.2901713(42) |
| $P_b^2$ | $2_{02}$ | B | 0.1619378(41) |
| $P_c^2$ | $2_{02}$ | C | 0.1012960(20) |
| $-P^4$ | $4_{04}$ | $\Delta_J$ | $0.11932(29)\times10^{-6}$ |
| $-P^2P_a^2$ | $4_{04}$ | $\Delta_{JK}$ | $0.869(22)\times10^{-7}$ |
| $-P_a^4$ | $4_{04}$ | $\Delta_K$ | $-0.2264(23)\times10^{-6}$ |
| $-2P^2(P_b^2-P_c^2)$ | $4_{04}$ | $\delta_j$ | $0.052615(145)\times10^{-6}$ |
| $-P_a^2,(P_b^2-P_c^2)$ | $4_{04}$ | $\delta_k$ | $0.13300(75)\times10^{-6}$ |
| $\{P_a,P_b\}$ | $2_{02}$ | $D_{ab}$ | $-0.440125(60)\times10^{-1}$ |
| $(1/2)\{P_a,P_b\}(1-\cos(3\alpha))$ | $4_{22}$ | $V_{3ab}$ | $-0.39134(64)\times10^{-2}$ |
| $P^2(1-\cos(3\alpha))$ | $4_{22}$ | $V_{3J}$ | $-0.9731(23)\times10^{-3}$ |
| $P_a^2(1-\cos(3\alpha))$ | $4_{22}$ | $V_{3K}$ | $0.14265(66)\times10^{-2}$ |
| $(P_b^2-P_c^2)(1-\cos(3\alpha))$ | $4_{22}$ | $V_{3bc}$ | $-0.9959(58)\times10^{-3}$ |
| $(1/2)\{P_a,(P_b^2-P_c^2)\}p_\alpha$ | $4_{13}$ | $\rho_{bc}$ | $0.981(12)\times10^{-6}$ |
| $(1/2)\{P_a,P_b\}P^2$ | $4_{04}$ | $D_{abJ}$ | $-0.652(12)\times10^{-7}$ |
| $(1/2)\{P_a^3,P_b\}(1-\cos(3\alpha))$ | $6_{24}$ | $0.5V_{3abK}$ | $-0.1080(41)\times10^{-6}$ |
| $P^6$ | $6_{06}$ | $\Phi_J$ | $-0.1186(51)\times10^{-14}$ |
| $P_a^6$ | $6_{06}$ | $\Phi_K$ | $0.3145(30)\times10^{-12}$ |
| $p_\alpha^3P_a$ | $4_{31}$ | $\rho_m$ | $-0.1738(34)\times10^{-3}$ |
| $p_\alpha^2(P_b^2-P_c^2)$ | $4_{22}$ | $F_{bc}$ | $-0.1272(18)\times10^{-4}$ |
| $(1/2)\{P_a^3,P_b\}$ | $4_{04}$ | $D_{abK}$ | $0.393(12)\times10^{-7}$ |
| | | N lines (A/E) | 1660/1627 |
| | | $J_{max}/K_{max}$ | 84/28 |
| | | RMS (MHz) | 0.0477 |
| | | WRMS | 0.933 |

[a] $n=t+r$, with $n$ the total order of the operator, $t$ the order of the torsional part and $r$ the order of the rotational part.
[b] All values are in $cm^{-1}$ except $\rho$ (unitless) and uncertainties are given in parenthesis in units of the last two digits ($1\sigma$).
[c] Fixed; estimated from the MP2/aVQZ equilibrium structure.

ies of $^bQ$-type transitions were introduced while freeing the appropriate parameters.

### 3.1.4. Final fit

3287 transitions, including 1660 and 1627 A and E components, respectively, from three different experiments (46 from FP-FTMW, 50 from [3] and 3191 from (sub-)mm-wave), with $J$ and $K_a$ values up to 84 and 28, respectively, have been fitted to experimental accuracy. Due to strong correlations, $F$ parameter has to be kept fixed to a value derived from the MP2/aVQZ equilibrium structure. The list of resulting parameters is shown in Table 1 together with their corresponding operators. The list of fitted lines with (obs-calc) values is provided in the supplementary material.

## 3.2. Study of the two lowest excited states

MG displays two low lying vibrational modes of $A''$ symmetry: the C-$CH_3$ torsion (internal rotation) $\nu_{20}$ around 120 $cm^{-1}$ and the internal C—C torsion (skeleton torsion) $\nu_{21}$ around 90 $cm^{-1}$. These two states are thus populated enough at room temperature for their rotational lines to be observed on the mm-wave spectrum, as can be seen on Fig. 4. Starting from transitions of the GS with low $K_a$ values only and including lines from $v_{20}=1$, fits have been performed using RAM36. GS and ES rotational lines up to $K_a=3$ only were reproduced close to experimental accuracy in a very effective fit. Indeed, compared to GS lines only fit, $V_3$ parameter change in ($GS+v_{20}=1$) lines fit was considered too important and $V_6$ parameter value was much larger than the usually expected value of about −3 % of $V_3$. In addition, attempts to fit the other lines cluster satellites (*i.e.* $v_{21}=1$) were unsuccessful as well. The list of observed lines is provided in the supplementary material.

## 3.3. Comparison with supporting quantum chemistry calculations

### 3.3.1. Excited states

An explanation for these fitting difficulties is evidenced by the harmonic force field calculations at the MP2/aVQZ level. Table 2 displays the atomic displacements associated with $\nu_{20}$ and $\nu_{21}$ normal modes. As expected for these two torsions (out-of-plane), H atoms have the most significants displacements. It can be seen that the absolute values of amplitudes are very close in both modes, making MG an extreme case with its two lowest vibrational normal modes $\nu_{20}$ and $\nu_{21}$ represented by a strong mixing between methyl and skeleton torsions, two internal motions very different in nature. In addition, the displacement of the two oxygen atoms in the same direction, opposite to carbon atoms #1 and #3, shows that the out-of-plane bends are also involved in these two normal modes. Although excited states lines were not fitted to the instru-

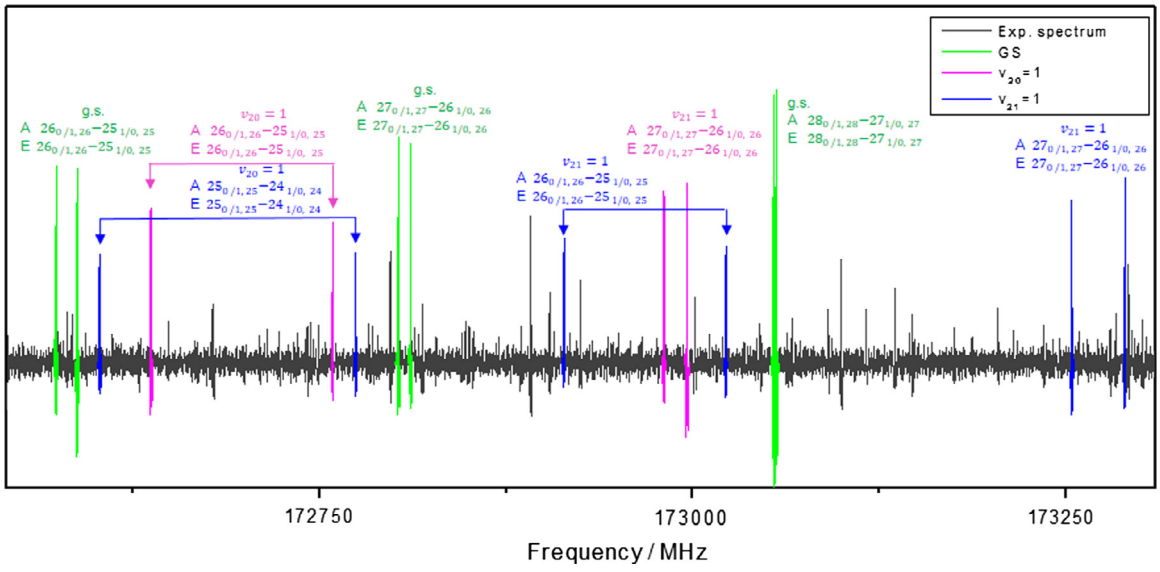


**Fig. 4.** Part of the mm-wave spectrum of *trans*-Methylglyoxal around 173 GHz. Ground state rotational lines (in green) are observed together with rotational lines from $v_{20}=1$ (in magenta) and $v_{21}=1$ (in blue). Assignments are in the format $J'_{K'_aK'_c}-J''_{K''_aK''_c}$. (For interpretation of the references to color in this figure legend, the reader is referred to the web version of this article.)

**Table 2**
Calculated atomic displacements (MP2/aVQZ) along the $\nu_{21}$ and $\nu_{20}$ normal modes of *trans*-Methylglyoxal.

| Atom | #[a] | $\nu_{21}$ | | | $\nu_{20}$ | | |
|---|---|---|---|---|---|---|---|
| | | X | Y | Z | X | Y | Z |
| C | 1 | −0.00 | −0.00 | 0.11 | 0.00 | 0.00 | 0.19 |
| H | 2 | −0.00 | 0.00 | 0.35 | 0.00 | −0.00 | 0.49 |
| C | 3 | 0.00 | −0.00 | 0.03 | −0.00 | 0.00 | 0.06 |
| C | 4 | 0.00 | 0.00 | 0.03 | −0.00 | −0.00 | 0.05 |
| H | 5 | 0.02 | 0.46 | 0.33 | 0.00 | −0.42 | −0.23 |
| H | 6 | −0.02 | −0.46 | 0.33 | −0.00 | 0.42 | −0.23 |
| H | 7 | −0.00 | 0.00 | −0.46 | 0.00 | −0.00 | 0.47 |
| O | 8 | −0.00 | −0.00 | −0.12 | 0.00 | 0.00 | −0.11 |
| O | 9 | 0.00 | −0.00 | −0.04 | −0.00 | 0.00 | −0.14 |

[a] See Fig. 3 for atom numbering.

mental accuracy, assignments of the dataset collected in the present study seem reliable and might be helpful in a future development of a model taking into account such a mixing of internal motions.

### 3.3.2. Methyl torsion potential energy curve

The height of the barrier to internal rotation of the methyl group has been estimated at the MP2/aVQZ level using the QST2 method as implemented in Gaussian09, leading to values of 250.4 $cm^{-1}$ and 280.5 $cm^{-1}$, without and with ZPE correction, respectively. These values agree very well with $V_3$ = 271.718 $cm^{-1}$ extracted from the fit of GS lines. To go beyond this only two energy points comparison, the MP2/aVQZ potential energy curve (PEC) along the torsional angle has been calculated by mean of a relaxed scan procedure along O—C—C—H dihedral angle with 5° steps. Three PEC are compared in Fig. 5. The MP2/aVQZ PEC is plotted in blue dots. It is difficult to apply a ZPE correction to a PEC. However, once this correction is known at the transition state (30.1 $cm^{-1}$ from the QST2 calculation), it can be applied relatively to each energy point of the curve. The ZPE corrected MP2/aVQZ PEC is plotted in red diamonds. An experimental PEC can be calculated from $V_3$ and $V_6$ values extracted from the fit as follows:

$$V_\alpha = \frac{V_3}{2}(1-\cos(3\alpha)) + \frac{V_6}{2}(1-\cos(6\alpha)) \quad (2)$$

where α is the torsional angle.

The PEC using $V_3$ from the fit of GS lines (with $V_6$ = 0 here) is plotted in green squares.

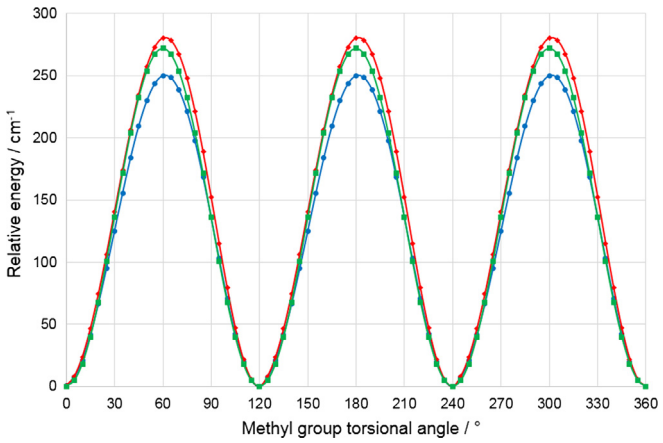


**Fig. 5.** Potential energy curves along the methyl group torsional angle of *trans*-Methylglyoxal: MP2/aVQZ in blue dots; ZPE corrected MP2/aVQZ in red diamonds; from Eq. (2) using $V_3$ from the fit of GS lines in green squares. See text for details. (For interpretation of the references to color in this figure legend, the reader is referred to the web version of this article.)

**Table 3**
Comparison between experimental and calculated rotational constants of *trans*-Methylglyoxal. Values are in MHz.

| | Exp. (RAM)[a] | $\Delta_1$[b] | $\Delta_2$[c] | $\Delta_3$[d] |
|---|---|---|---|---|
| A | 9104.10 | −80.85 | 18.03 | 17.90 |
| B | 4441.58 | −21.00 | 3.60 | 1.03 |
| C | 3041.07 | −17.95 | 5.97 | 5.97 |

[a] Constants from the fit of GS lines using RAM36.
[b] Difference between experimental and equilibrium MP2/CBS PAM constants.
[c] Difference between experimental and PAM hybrid constants.
[d] Difference between experimental and RAM hybrid constants (see text for details).

As can be seen from Fig. 5, PECs ZPE corrected and from the GS lines fit are in very good agreement, the slight shift observed at the descending side of the calculated curves being most probably due to a too large grid step and being in any case within an expected error of several $cm^{-1}$. This tends to consolidate the quality of the GS lines fit and, in turn, to validate the procedure of applying a relative ZPE correction to the bare electronic energy curve.

### 3.3.3. GS rotational constants

They represent the most direct parameters to be compared between the two independent ways that are fits and calculations. However, rotational constants are calculated at equilibrium while adjusted experimentally to values in a given vibrational state, so vibrational contribution to calculated values shall be included by any mean to be reasonably compared to experimental values. In the present case, vibrational contribution has been included with the "hybrid" method (see Eq. (1) and [18]). In addition, when taking into account an internal rotor, experimental constants are expressed in the RAM system while calculated constants are expressed in the PAM system. However, calculated constants can be converted into the RAM system using Herschbach formalism [26]. A step by step comparison between experimental and calculated constants is shown in Table 3. $\Delta_i$ represent the difference between experimental constants from the RAM36 fit of GS lines and calculated constants: $i$ = 1 MP2/CBS at equilibrium, $i$ = 2 in the GS applying the "hybrid" correction and $i$ = 3 GS "hybrid" in the RAM system. As expected, the vibrational correction has the most significant effect by decreasing the discrepancies by a factor of about 4. The PAM to RAM conversion is less significant but tends to decrease slightly the overestimated "hybrid" values. Finally, this excellent agreement (discrepancies less than 0.2 %) represent another inter-validation of the experimental and theoretical results.

## 4. Conclusion

The rotational spectrum of *trans*-Methylglyoxal in its vibrational ground state has been recorded and fitted to the experimental accuracy. In addition to the early cm-wave study [3], lines in the cm-wave, mm-wave and submm-wave regions have been included and the methyl group internal rotation has been taken into account in the model. Data and parameters are reliable, as shown by the good agreement between experiments and calculations, and can be used in atmospheric models or for a detection of Methylglyoxal in the interstellar medium. Fits of observed rotational lines in the two lowest excited states were unsuccessful, most probably due to a very strong mixing of the two internal motions, as suggested by the supporting quantum chemistry calculations. However, the dataset collected in the present study might be helpful in a future development of a model taking into account such a mixing.

## Acknowledgments

The present work was funded by the French ANR "Labex CaPPA" through the PIA under contract ANR-11-LABX-0005-01, by the Regional Council *Hauts-de-France*, by the European Funds for Regional Economic Development (FEDER) and by the Ministère de l'Enseignement Supérieur et de la Recherche – France (CPER Climibio). S.B. acknowledges the Regional Council *Hauts-de-France* for the financial support of her Ph.D. thesis.

## Appendix A. Supplementary material

The supplementary material contains: The list of fitted lines with (obs-calc) values for the vibrational ground state of *trans*-Methylglyoxal; the list of observed lines for the $v_{20} = 1$ and $v_{21} = 1$ vibrational excited states of *trans*-Methylglyoxal. Supplementary data associated with this article can be found, in the online version, at https://doi.org/10.1016/j.jms.2017.12.007.

## References

[1] T.-M. Fu, D.J. Jacob, F. Wittrock, J.P. Burrows, M. Vrekoussis, D.K. Henze, Global budgets of atmospheric glyoxal and methylglyoxal, and implications for formation of secondary organic aerosols, J. Geophys. Res.: Atmos. 113 (D15) (2008) D15303, https://doi.org/10.1029/2007JD009505.

[2] P.A. Akishin, L.V. Viikov, N.I. Mochalova, Electron-diffraction study of the structure of molecules with conjugated double bonds, J. Struct. Chem. 2 (5) (1961) 505–509, https://doi.org/10.1007/BF00746506.

[3] C. Dyllick-Brenzinger, A. Bauder, Microwave spectrum, dipole moment and barrier to internal rotation of trans-methyl glyoxal, Chem. Phys. 30 (2) (1978) 147–153, https://doi.org/10.1016/0301-0104(78)85114-3.

[4] L.T.M. Profeta, R.L. Sams, T.J. Johnson, S.D. Williams, Quantitative infrared intensity studies of vapor-phase glyoxal, methylglyoxal, and 2,3-butanedione (diacetyl) with vibrational assignments, J. Phys. Chem. A 115 (35) (2011) 9886–9900, https://doi.org/10.1021/jp204532x.

[5] O. Zakharenko, R.A. Motiyenko, J.-R.A. Moreno, A. Jabri, I. Kleiner, T.R. Huet, Torsion-rotation-vibration effects in the ground and first excited states of methacrolein, a major atmospheric oxidation product of isoprene, J. Chem. Phys. 144 (2) (2016) 024303, https://doi.org/10.1063/1.4939636.

[6] O. Zakharenko, R.A. Motiyenko, J.R.A. Moreno, T.R. Huet, Conformational landscape and torsion-rotation-vibration effects in the two conformers of methyl vinyl ketone, a major oxidation product of isoprene, J. Phys. Chem. A, doi:https://doi.org/10.1021/acs.jpca.7b06360.

[7] T.J. Balle, W.H. Flygare, Fabryperot cavity pulsed fourier transform microwave spectrometer with a pulsed nozzle particle source, Rev. Scient. Instrum. 52 (1) (1981) 33–45, https://doi.org/10.1063/1.1136443.

[8] J. Grabow, W. Stahl, H. Dreizler, A multioctave coaxially oriented beam-resonator arrangement Fourier-transform microwave spectrometer, Rev. Scient. Instrum. 67 (12) (1996) 4072–4084, https://doi.org/10.1063/1.1147553.

[9] J.-U. Grabow, Fourier transform microwave spectroscopy measurement and instrumentation, in: M. Quack, F. Merkt (Eds.), Handbook of High-Resolution Spectroscopy, vol. 2, John Wiley & Sons, Ltd, 2011, pp. 723–799.

[10] S. Kassi, D. Petitprez, G. Wlodarczak, Microwave fourier transform spectroscopy of t-butylchloride and t-butylbromide isotopic species, J. Mol. Struct. 517–518 (2000) 375–386, https://doi.org/10.1016/S0022-2860(99)00296-3.

[11] M. Tudorie, L.H. Coudert, T.R. Huet, D. Jegouso, G. Sedes, Magnetic hyperfine coupling of a methyl group undergoing internal rotation: a case study of methyl formate, J. Chem. Phys. 134 (7) (2011) 074314, https://doi.org/10.1063/1.3554419.

[12] S. Kassi, D. Petitprez, G. Wlodarczak, Microwave spectrum of isotopic species of urea $(NH_2)_2CO$, J. Mol. Spectrosc. 228 (2) (2004) 293–297, https://doi.org/10.1016/j.jms.2004.05.002.

[13] O. Zakharenko, R.A. Motiyenko, L. Margulès, T.R. Huet, Terahertz spectroscopy of deuterated formaldehyde using a frequency multiplication chain, J. Mol. Spectrosc. 317 (2015) 41–46.

[14] M.J. Frisch, G.W. Trucks, H.B. Schlegel, G.E. Scuseria, M.A. Robb, J.R. Cheeseman, G. Scalmani, V. Barone, B. Mennucci, G.A. Petersson, H. Nakatsuji, M. Caricato, X. Li, H.P. Hratchian, A.F. Izmaylov, J. Bloino, G. Zheng, J.L. Sonnenberg, M. Hada, M. Ehara, K. Toyota, R. Fukuda, J. Hasegawa, M. Ishida, T. Nakajima, Y. Honda, O. Kitao, H. Nakai, T. Vreven, J.A. Montgomery Jr., J.E. Peralta, F. Ogliaro, M. Bearpark, J.J. Heyd, E. Brothers, K.N. Kudin, V.N. Staroverov, R. Kobayashi, J. Normand, K. Raghavachari, A. Rendell, J.C. Burant, S.S. Iyengar, J. Tomasi, M. Cossi, N. Rega, J.M. Millam, M. Klene, J.E. Knox, J.B. Cross, V. Bakken, C. Adamo, J. Jaramillo, R. Gomperts, R.E. Stratmann, O. Yazyev, A.J. Austin, R. Cammi, C. Pomelli, J.W. Ochterski, R.L. Martin, K. Morokuma, V.G. Zakrzewski, G.A. Voth, P. Salvador, J.J. Dannenberg, S. Dapprich, A.D. Daniels, O. Farkas, J.B. Foresman, J.V. Ortiz, J. Cioslowski, D.J. Fox, Gaussian 09 Revision D.01, Gaussian Inc., Wallingford, CT, 2009.

[15] R.A. Kendall, T.H. Dunning Jr., R.J. Harrison, Electron affinities of the first row atoms revisited. Systematic basis sets and wave functions, J. Chem. Phys. 96 (9) (1992) 6796–6806, https://doi.org/10.1063/1.462569.

[16] D.E. Woon, T.H. Dunning Jr., Benchmark calculations with correlated molecular wave functions. vi. Second row a2 and first row/second row ab diatomic molecules, J. Chem. Phys. 101 (10) (1994) 8877–8893, https://doi.org/10.1063/1.468080.

[17] V. Barone, Anharmonic vibrational properties by a fully automated second-order perturbative approach, J. Chem. Phys. 122 (1) (2005) 014108, https://doi.org/10.1063/1.1824881.

[18] M. Biczysko, P. Panek, G. Scalmani, J. Bloino, V. Barone, Harmonic and anharmonic vibrational frequency calculations with the double-hybrid b2plyp method: analytic second derivatives and benchmark studies, J. Chem. Theory Comput. 6 (7) (2010) 2115–2125, https://doi.org/10.1021/ct100212p.

[19] S. Grimme, M. Steinmetz, Effects of London dispersion correction in density functional theory on the structures of organic molecules in the gas phase, Phys. Chem. Chem. Phys. 15 (2013) 16031–16042, https://doi.org/10.1039/C3CP52293H.

[20] M. Goubet, P. Soulard, O. Pirali, P. Asselin, F. Real, S. Gruet, T.R. Huet, P. Roy, R. Georges, Standard free energy of the equilibrium between the trans-monomer and the cyclic-dimer of acetic acid in the gas phase from infrared spectroscopy, Phys. Chem. Chem. Phys. 17 (2015) 7477–7488, https://doi.org/10.1039/C4CP05684A.

[21] O. Pirali, M. Goubet, V. Boudon, L. DÁccolti, C. Fusco, C. Annese, Characterization of isolated 1-aza-adamantan-4-one ($C_9H_{13}NO$) from microwave, millimeter-wave and infrared spectroscopy supported by electronic structure calculations, J. Molec. Spectrosc. 338 (2017) 6–14, https://doi.org/10.1016/j.jms.2017.04.020.

[22] H.M. Pickett, The fitting and prediction of vibration-rotation spectra with spin interactions, J. Mol. Spectrosc. 148 (2) (1991) 371–377, https://doi.org/10.1016/0022-2852(91)90393-O.

[23] H. Hartwig, H. Dreizler, The microwave spectrum of trans-2,3-dimethyloxirane in torsional excited states, Z. Naturforsch 51a (8) (1996) 923–932, https://doi.org/10.1515/zna-1996-0807.

[24] V.V. Ilyushin, Z. Kisiel, L. Pszczòkowski, H. Mader, J.T. Hougen, A new torsion-rotation fitting program for molecules with a sixfold barrier: application to the microwave spectrum of toluene, J. Molec. Spectrosc. 259 (1) (2010) 26–38, https://doi.org/10.1016/j.jms.2009.10.005.

[25] V. Ilyushin, R. Rizzato, L. Evangelisti, G. Feng, A. Maris, S. Melandri, W. Caminati, Almost free methyl top internal rotation: rotational spectrum of 2-butynoic acid, J. Molec. Spectrosc. 267 (1) (2011) 186–190, https://doi.org/10.1016/j.jms.2011.03.028.

[26] D.R. Herschbach, Calculation of energy levels for internal torsion and overall rotation. iii, J. Chem. Phys. 31 (1) (1959) 91–108, https://doi.org/10.1063/1.1730343.